



FIB/SEM-based calculation of tortuosity in a porous LiCoO₂ cathode for a Li-ion battery

T. Hutzenlaub ^{a,*}, A. Asthana ^c, J. Becker ^b, D.R. Wheeler ^c, R. Zengerle ^a, S. Thiele ^a

^a Laboratory for MEMS Applications, IMTEK – Department of Microsystems Engineering, University of Freiburg, Georges-Koehler-Allee 103, 79110 Freiburg, Germany

^b Fraunhofer Institute for Industrial Mathematics (ITWM), Fraunhofer-Platz 1, 67663 Kaiserslautern, Germany

^c Department of Chemical Engineering, Brigham Young University, 350 CB Provo, UT 84602, United States

ARTICLE INFO

Article history:

Received 22 October 2012

Received in revised form 7 November 2012

Accepted 7 November 2012

Available online 17 November 2012

Keywords:

Three-dimensional reconstruction

Li-ion battery cathode

Tortuosity

Porous media

Pore size distribution

Bruggeman equation

ABSTRACT

We present a new method to quantify tortuosity in the porous, LiCoO₂ cathode of a Li-ion battery. The starting point is a previously published 3D reconstruction from FIB/SEM images with three phases, the active material domain, carbon-binder domain and pore space. Based on this geometrical configuration, we compute effective diffusivities, from which we in turn derive tortuosity values for the pore space ranging between 5 and 11.6 for the three spatial directions. In a next step, we compare our approach to an imaging method that employs back-filling material. These methods do not differentiate between the carbon-binder domain and the pore space. Thus we remove the carbon-binder domain from our 3D reconstruction and add its volume to the pore space. As a result of this procedure, the tortuosity is greatly reduced to values between 1.5 and 1.9. Experiments suggest that both results for tortuosity are inaccurate and that the real values lie somewhere between these parameter sets. Hence, based on experimental data, we propose a nanoporous carbon-binder domain and derive intermediate tortuosity values between 4.2 and 6.1. These values are consistent with experimental values for similar Li-ion cathodes reported previously.

© 2012 Elsevier B.V. All rights reserved.

1. Introduction

Tortuosity is one of the most important parameters to characterize a porous medium, allowing it to be included in a macro-homogeneous model without describing the complete, complex pore structure [1]. In the past, the most common approach to calculate tortuosity was to apply the Bruggeman equation [1,2] and thus express the tortuosity τ as a function of the porosity ε :

$$\tau = \varepsilon^{1-\alpha} \quad (1)$$

α is defined as the Bruggeman exponent. It has been shown that $\alpha \approx 1.5$ is an appropriate value to describe the pore volume of a packing of equally sized spheres [3,4]. This value is often used in simulations to model transport properties of Li-ion batteries. However, its accuracy to describe the real microstructure has been doubted. Some researchers have thus used higher values for α [1,5,6] or added an additional factor γ [7,8] to adjust the tortuosity. Thorat et al. [9] also introduced an experimental method to measure the tortuosity in Li-ion batteries by combining AC impedance and polarization-interrupt methods.

Wilson et al. [10] employed focused ion-beam scanning/electron microscopy (FIB/SEM) [11] to study the porous microstructure in solid oxide fuel cells. This method was later extended to polymer electrolyte

membrane fuel cells [12,13]. It provides the basis for three-dimensional representations of a porous medium by alternately removing thin layers of material and imaging the surface. Subsequently, a segmentation step is carried out to differentiate between pores and the solid phase. Ender et al. reconstruct the LiFePO₄ cathode of a Li-ion battery [14]. This technique was also utilized to study the LiCoO₂ cathode of a Li-ion battery by first infiltrating the sample with backfilling material [15]. The morphology and distribution of the active-material domain, which mainly consists of LiCoO₂ particles, could be clearly identified. This comes at the cost of no contrast and consequently no differentiation between the pore space and the carbon-binder domain.

In prior work of our group, the LiCoO₂ cathode of a Li-ion battery was reconstructed from FIB/SEM images without using a backfilling material [16]. After a subsequent semi-automatic segmentation step, it became possible to differentiate between the three constituents: active material domain, carbon-binder domain and pore space.

In the work reported now, we utilize this three-phase morphology to quantify pore space tortuosity in all three spatial directions. We compare these results to values that are calculated by methods which do not differentiate between the carbon-binder domain and the pore space. Additionally, we present a new tomographic method for LiCoO₂ cathodes of Li-ion batteries, utilizing experimental data generated by Stephenson et al. [17]. With this method, we derive more realistic tortuosity values that take into account the presence of nanopores in the carbon-binder domain which cannot be imaged by the FIB/SEM resolution employed.

* Corresponding author. Tel.: +49 76120373269; fax: +49 76120373299.

E-mail address: tobias.hutzenlaub@imte.de (T. Hutzenlaub).

2. Image processing

The starting point for the calculations in this work is the three-dimensional reconstruction of a LiCoO_2 cathode for a Li-ion battery that was first published in [16]. This reconstruction is represented as a stack of 200 images, where pore space, active material and the carbon-binder domain are depicted by three different gray-scale values (Fig. 1a). The intermediate gray value represents distinct and relatively homogeneous domains that contain a combination of carbon, binder, and nanoscale pores, as has previously been observed for other porous Li-ion electrodes [17]. Each image consists of pixels with a resolution of $35 \text{ nm} \times 35 \text{ nm}$ (x and y directions; the y direction is the through-plane direction, perpendicular to the electrode surface). The average distance between images is 62 nm (z direction). The total reconstruction measures $20.02 \mu\text{m} \times 18.13 \mu\text{m} \times 12.4 \mu\text{m}$, which is equivalent to $572 \times 518 \times 200$ anisotropic voxels. The resolution chosen was a trade-off between the size of LiCoO_2 particles which could be resolved and acquisition time.

Most of the calculations were performed with GeoDict [18], which made it necessary to resample the given geometrical structure to create isotropic voxels. This was achieved by employing the majority wins algorithm with the software ScanIP [19] to create a geometrical representation consisting of $646 \times 585 \times 400$ isotropic voxels. The new

edge length of one voxel is 31 nm. This 3D representation is referred to as “Model A” in the following text.

Finally, the carbon-binder domain was removed by adding all its voxels to the pore space by applying an appropriate threshold. This created a second geometrical representation, allowing comparison to methods which do not differentiate between the carbon-binder domain and the pore space (Fig. 1b). This 3D representation is referred to as “Model B”.

3. Methods and results

3.1. Pore size distribution

In a first step, we compare the pore size distributions of Model A and Model B. The pore size distribution is calculated by using a method first described by Delerue et al. [20] with GeoDict [18] (Fig. 2a). The pore size distribution of Model A peaks in the lowest pore diameter interval investigated. As one would expect a more even distribution in the real microstructure, this indicates that there is a considerable number of pores that are too small to be imaged with the FIB/SEM resolution employed. The pore size distribution of Model B peaks at approximately $1 \mu\text{m}$, which is well within the range of pore sizes investigated. This is an indication that the method is well suited to image the active material phase. When the two distributions are compared, it is evident that

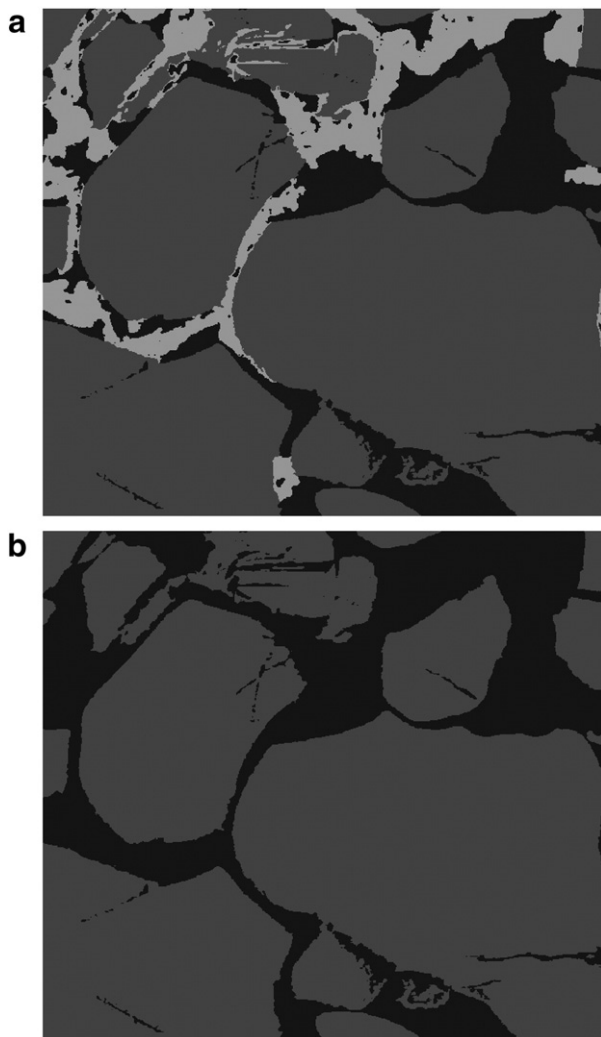


Fig. 1. a) A segmented image of the 3D representation used in this work. The three phases can be distinguished according to their gray-scale value (active material domain = dark gray, carbon-binder domain = light gray, and pore space = black). b) The same image with the carbon-binder domain replaced by additional pore space.

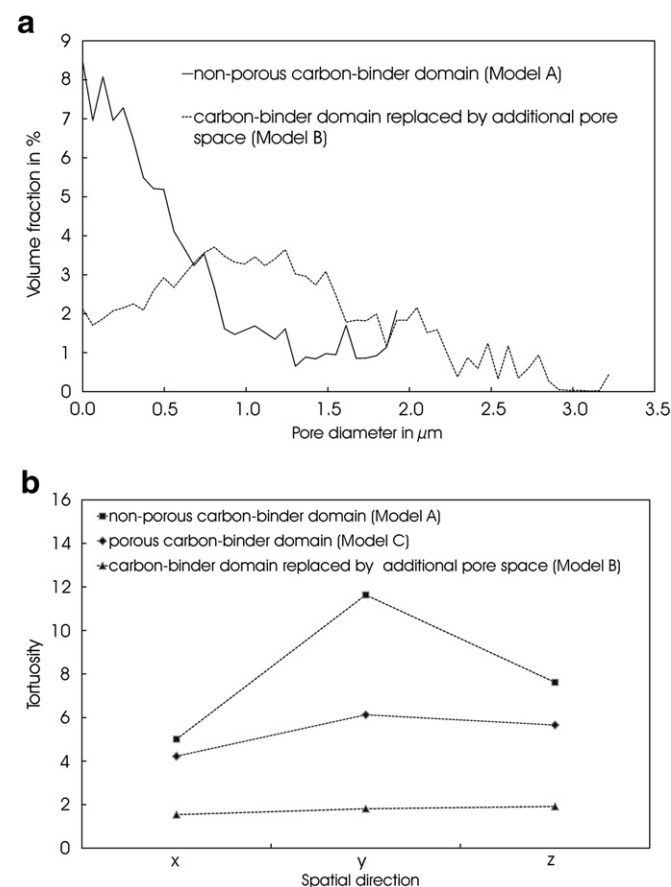


Fig. 2. a) Pore size distribution of the pore space in the original 3D reconstruction consisting of three phases and pore size distribution of the 3D reconstruction consisting of two phases, where the carbon-binder domain is replaced by additional pore space. b) Comparison of tortuosity values in all three spatial directions. Replacing the carbon-binder domain by additional pore space greatly reduces the tortuosity values and makes the results much more homogeneous (Model B). Differentiating between the non-porous carbon-binder domain and the pore space leads to the largest and most inhomogeneous tortuosity values (Model A). Based on experimental data, we propose a porous carbon-binder domain with a porosity of 65% which leads to intermediate, only slightly inhomogeneous tortuosity values (Model C). Connecting lines between data points are added as a guide to the eye.

the pores which are too small to be resolved must be situated in the carbon-binder domain. This conclusion is supported by the fact that nanosized carbon particles mixed with binder typically contain pores which are much smaller than the resolution employed in this investigation [21].

3.2. Volume distribution

The volume distribution of pore space, active material domain and carbon-binder domain of Models A and B is determined by counting the number of voxels representing each phase and then dividing this value by the total number of voxels in the 3D representation. GeoDict [18] is used as the calculation tool (Table 1).

3.3. Tortuosity

The tortuosity τ is described by:

$$\tau_{\kappa} = \frac{D^0 \varepsilon}{D_{\kappa}^{eff}} \quad \kappa = x, y, z \quad (2)$$

with D^0 defined as the intrinsic diffusivity of a substance in a gas, liquid or solid e.g. the diffusivity of Li ions in electrolyte. This intrinsic diffusivity is reduced to a so-called effective diffusivity D_{κ}^{eff} in a tortuous porous structure. The tortuosity of the porous medium is calculated as described by Becker et al. [22] with GeoDict [18] by first solving Laplace's equation numerically with the Li ion concentration c separately for each spatial direction:

$$-\Delta c_{\kappa} = 0 \quad \kappa = x, y, z. \quad (3)$$

In each case the result is a diffusion flux from which we derive D_{κ}^{eff} with Fick's law. With Eq. (2) we finally determine τ_{κ} . For Model A, we calculate tortuosity values between 5 and 11.6 depending on the spatial direction (Fig. 2b, Table 1). Adding the carbon-binder domain to the pore space (Model B) yields strongly reduced and more homogeneous tortuosity values between 1.5 and 1.9 (Fig. 2b, Table 1). It is noteworthy that these values for Model B best fit the well-known Bruggeman coefficient of 1.5 when inserted into Eq. (1).

3.4. Modeling a nanoporous carbon-binder domain

Pore size distributions as determined by this work suggest that a significant number of pores in the carbon-binder domain cannot be resolved in FIB/SEM images. This conclusion is additionally supported by experimental data generated by Stephenson et al. [17], which is based on volume conservation. To account for this, we create a new Model C. We do this by adding the following experimentally derived values taken directly from Stephenson et al. [17] to the carbon-binder domain of Model A: i) 65% porosity and ii) Li-ion diffusivity or conductivity of 5% compared to the pore space filled with electrolyte. Accordingly,

Table 1

Volume distribution of the three phases (active material domain, carbon-binder domain, and pore space domain) and tortuosity values calculated here. The three Models A, B and C differ in the definition of the carbon-binder domain. In Model A, the carbon-binder domain is regarded as a solid constituent. In Model B, it is removed and its volume is added to the pore space domain. In Model C, the carbon-binder domain is considered as porous material, dividing it into carbon-binder solids and a nanoporous space that is included to determine the total porosity.

		Model A	Model B	Model C
Volume distribution	Porosity	% 13.1	30.2	24.2
	Carbon-binder domain	% 17.1	0.0	6.0
	Active material domain	% 69.8	69.8	69.8
Tortuosity	x direction	5.0	1.5	4.2
	y direction (through-plane)	11.6	1.8	6.1
	z direction	7.6	1.9	5.7

the tortuosity calculation is performed with GeoDict [18] by assigning diffusivities of D^0 (pore space) and $0.05 D^0$ (carbon-binder domain) and solving for D_{κ}^{eff} . With Eq. (2) and the new total porosity of 24.2%, we calculate intermediate tortuosity values between 4.2 and 6.1 for the three spatial directions (Fig. 2b, Table 1). The calculated tortuosity values for Model C are now consistent with experimental values for similar (but not identical) Li-ion cathodes obtained previously [17].

4. Conclusion

We calculated tortuosity values for three different variants of the same 3D representation of a LiCoO₂ cathode for a Li-ion battery which was reconstructed from FIB/SEM images [16]. The three variants of the same 3D geometrical configuration differ in the model applied for the carbon-binder domain. On the one hand, replacing the carbon-binder domain by pore space (Model B) best emulates the situation when the morphology is reconstructed from imaging methods that rely on backfilling material and do not differentiate between the carbon-binder domain and the pore space. Only the distribution and morphology of the active material domain can be identified correctly in these approaches. Though the tortuosity results agree very well with the established Bruggeman coefficient of $\alpha \approx 1.5$, this geometrical variant is least similar to the real morphology of the cathode as it totally neglects the carbon-binder domain and displays a much higher porosity.

On the other hand, the geometrical variant which includes only those pores that can be resolved by FIB/SEM (Model A) leads to very high tortuosity values.

In order to gain a realistic picture of ion transport pathways, pores in the carbon-binder domain which are smaller than the resolution limit should be taken into account. Supported by experimental data, we suggest a nanoporous carbon-binder domain which leads to intermediate tortuosity values between 4.2 and 6.1. We recommend these values as being the most realistic for macro-homogeneous models. Tortuosity values corresponding to Models A and B can be considered to be legitimate upper and lower bounds to the true average tortuosity of this porous electrode.

List of symbols

c	concentration (mol m^{-3})
D_{κ}^{eff}	effective bulk diffusivity ($\text{m}^2 \text{s}^{-1}$)
D^0	free, substance-specific diffusivity ($\text{m}^2 \text{s}^{-1}$)
α	Bruggeman coefficient
γ	Bruggeman factor
ε	porosity
κ	subscript defining spatial direction
τ	tortuosity

References

- [1] M. Doyle, J. Newman, A.S. Gozdz, C.N. Schmutz, J.M. Tarascon, Journal of the Electrochemical Society 143 (1996) 1890.
- [2] D.A.G. Bruggeman, Annalen der Physik 416 (1935) 665.
- [3] R.B. MacMullin, G.A. Muccini, AIChE Journal 2 (1956) 393.
- [4] R.E. De La Rue, C.W. Tobias, Journal of the Electrochemical Society 106 (1959) 827.
- [5] D. Djian, F. Alloin, S. Martinet, H. Lignier, J.Y. Sanchez, Journal of Power Sources 172 (2007) 416.
- [6] K.K. Patel, J.M. Paulsen, J. Desilvestro, Journal of Power Sources 122 (2003) 144.
- [7] K.M. Abraham, Electrochimica Acta 38 (1993) 1233.
- [8] D.E. Stephenson, E.M. Hartman, J.N. Harb, D.R. Wheeler, Journal of the Electrochemical Society 154 (2007) A1146.
- [9] I.V. Thorat, D.E. Stephenson, N.A. Zacharias, K. Zaghbi, J.N. Harb, D.R. Wheeler, Journal of Power Sources 188 (2009) 592.
- [10] J.R. Wilson, W. Kobsiriphat, R. Menziona, H.Y. Chen, J.M. Hiller, D.J. Miller, K. Thornton, P.W. Voorhees, S.B. Adler, S.A. Barnett, Natural Materials 5 (2006) 541.
- [11] L. Holzer, F. Indutnyi, P.H. Gasser, B. Munch, M. Wegmann, Journal of Microscopy 216 (2004) 84.
- [12] C. Ziegler, S. Thiele, R. Zengerle, Journal of Power Sources 196 (2011) 2094.

- [13] S. Thiele, R. Zengerle, C. Ziegler, *Nano Research* 4 (2011) 849.
- [14] M. Ender, J. Joos, T. Carraro, E. Ivers-Tiffée, *Electrochemistry Communications* 13 (2011) 166.
- [15] J.R. Wilson, J.S. Cronin, S.A. Barnett, S.J. Harris, *Journal of Power Sources* 196 (2011) 3443.
- [16] T. Hutzenlaub, S. Thiele, R. Zengerle, C. Ziegler, *Electrochemical and Solid-State Letters* 15 (2012) A33.
- [17] D.E. Stephenson, B.C. Walker, C.B. Skelton, E.P. Gorzkowski, D.J. Rowenhorst, D.R. Wheeler, *Journal of the Electrochemical Society* 158 (2011) A781.
- [18] www.geodict.com, 2012.
- [19] www.simpleware.com, 2012.
- [20] J.F. Delerue, E. Perrier, Z.Y. Yu, B. Velde, *Physics and Chemistry of the Earth Part A – Solid Earth and Geodesy* 24 (1999) 639.
- [21] T. Soboleva, X. Zhao, K. Malek, Z. Xie, T. Navessin, S. Holdcroft, *Applied Materials & Interfaces* 2 (2010) 375.
- [22] J. Becker, C. Wieser, S. Fell, K. Steiner, *International Journal of Heat and Mass Transfer* 54 (2011) 1360.